HHS Public Access

Author manuscript

Anal Chem. Author manuscript; available in PMC 2015 August 11.

Published in final edited form as:

Anal Chem. 2013 February 19; 85(4): 2183–2190. doi:10.1021/ac303531y.

Silver Clusters as both Chromophoric Reporters and DNA Ligands

Jeffrey T. Petty[*,#,‡], **Banabihari Giri**[‡], **Ian C. Miller**, **David A. Nicholson**, **Orlin O. Sergev**, **Taylor M. Banks**, and **Sandra P. Story**

Department of Chemistry, Furman University, Greenville, SC 29613

Abstract

Molecular silver clusters conjugated with DNA act as analyte sensors. Our studies evaluate a type of cluster-laden DNA strand whose structure and silver stoichiometry changes with hybridization. The sensor strand integrates two functions: the 3′ region binds target DNA strands through base recognition while the 5′ sequence $C_3AC_3AC_3TC_3A$ favors formation of a near infrared absorbing and emitting cluster. This precursor form exclusively harbors an ~11 silver atom cluster that absorbs at 400 nm and that condenses its single-stranded host. The 3′ recognition site associates with a complementary target strand, thereby effecting a 330 nm red-shift in cluster absorption and a background-limited recovery of cluster emission at 790 nm. One factor underlying these changes is sensor unfolding and aggregation. Variations in salt and oligonucleotide concentrations control cluster development by influencing DNA association. Structural studies using fluorescence anisotropy, fluorescence correlation spectroscopy, and size exclusion chromatography show that the sensor-cluster conjugate opens and subsequently dimerizes with hybridization. A second factor contributing to the spectral and photophysical changes is cluster transformation. Empirical silver stoichiometries are preserved through hybridization, so hybridized, dimeric near infrared conjugates host twice the amount of silver in relation to their violet absorbing predecessors. These DNA structure and net silver stoichiometry alterations provide insight into how DNA-silver conjugates recognize analytes.

Keywords

Silver Clusters; Biosensing; Fluorescence

Corresponding Author: jeff.petty@furman.edu, Phone: 864-294-2689.

[#]Henry Keith and Ellen Hard Townes Professor of Chemistry

[‡]These authors contributed equally.

Author Contributions

The manuscript was written through contributions of all authors. All authors have given approval to the final version of the manuscript.

Supporting Information:

The supporting information contains 8 figures describing spectra associated with alternate recognition sites, the Ag^+ stoichiometry associated with the violet-absorbing species, silver stoichiometry in the conjugates, the chromatographic isolation of the violet and near-infrared complexes, the relative target concentration in the hybridized sensor, the ionic and salt dependences of the cluster transformation, the chromatographic isolation of a dimer with two structurally distinct target, and the pH dependence of the cluster transformation. This material is available free of charge via the Internet at http://pubs.acs.org.

Sensors based on few-atom clusters of silver conjugated with DNA feature *convenient synthesis*, *fluorescence-based detection*, and *discriminate analyte responses*. Metallic clusters are created in aqueous solution via chemical reduction of cationic precursors, like their nanoparticle counterparts.[1–3] Growth is constrained by strongly coordinating ligands, as illustrated by DNA strands that direct formation of silver clusters with ~10 atoms.[4–17] Electron-rich sites in the nucleobases stabilize these small agglomerates, as shown by pH-dependent emission that correlates with N3 ionization, by coordination-induced shifts in the core electron energies of heteroatoms in DNA strands, and by favorable complexation with nitrogen functional groups.[5–8] Coordination with different nucleobases in these polymeric hosts dictates cluster formation when DNA-bound Ag^+ is reduced with BH_4^-.[11] Additionally, solution pH, oxygen concentrations, and temperature direct reaction outcome to favor specific clusters.[13,14,18,19] Thus, a key advantage of silver clusters as analyte sensors is that sequence-programmable reporters are conveniently synthesized in aqueous buffers using readily available reagents.

Another appealing aspect of DNA-bound silver clusters is their high molecular brightness due to fluorescence quantum yields of 10–70% and extinction coefficients from 100,000–350,000 $M^{-1}cm^{-1}$.[11,12,20] Radiative relaxation within the sparse density of electronic states is not only efficient but also sustained without intermittent blinking because emissive excited states are weakly coupled to dark electronic states, thereby enabling detection of single molecules.[21,22] Sensitivity and selectivity are further enhanced when secondary lasers modulate fluorescence by redirecting population back to the emissive manifold of states. [23,24] Silver-based chromophores are particularly distinguished in the near infrared spectral region where organic dyes have low fluorescence quantum yields in water and semiconductor nanocrystals are typically large (10 – 40 nm) to achieve small band gaps.[25,26] An example is an ~10 atom cluster with λ_{ex} = 750 nm and λ_{em} = 810 nm that forms with $C_3AC_3AC_3TC_3A$.[27] Optical detection in the near infrared is favored because scattering is reduced relative to shorter wavelengths, light absorption by hemoglobin, lipids, and water is minimized, and background autofluorescence from endogenous chromophores is largely eliminated.[28,29] A resulting lower background combined with the inherent brightness of silver cluster fluorophores facilitates sensitive detection in complex samples.[27,30–32] Furthermore, optically-based analysis is also attractive because near infrared emitting diode lasers are commercially available for selective cluster excitation.[33]

The foundation of silver cluster-based detection lies in how analytes modulate the environments of DNA-bound clusters. Two general concepts provide a framework for interpreting how nucleic acids, proteins, and inorganic cations are identified through their association with cluster-laden DNA strands.[30,34–40] First, analytes that change DNA structure in turn alter cluster binding sites. As examples, allosteric changes induced by mismatched base pairs extinguish distantly-located yellow emitting clusters, proximal positioning of DNA strands influences both the emission rate and spectrum of DNA-bound clusters, pH guides the assembly of multistranded DNA hosts for red- and green-emitting clusters, and structural changes in aptamers propagate to DNA-appended red-emitting clusters.[13,31,34,37,41,42] These changes may reflect alterations in a delicate network of coordination by multiple nucleobases.[13,14] Second, new silver species form in response to

particular DNA environments. Cluster evolution is revealed by fluorescence lifetime measurements that study static quenching and by fluorescence correlation spectroscopy that enumerates emitting clusters. Supporting examples of analyte-driven cluster transformation include amplification in the number of red emitting clusters when a cluster-DNA conjugate is positioned next to a guanine-rich strand, a loss of emissive clusters when thrombin and Hg^{2+} associate with their respective sensors, and an increase in number of clusters emitters when hybridization exposes new binding sites for near-infrared emitting conjugates.[37,39,43,30]

In this work, specific DNA sequences are identified by altering the environments of DNA-bound silver clusters. Oligonucleotides are analyzed because the strength and specificity of complementary interactions allows attention to be directed to understanding the sensor/cluster interaction. Target hybridization transforms the cluster environment, as absorption shifts from the violet to near infrared and strong near infrared emission develops (Fig. 1). Our studies consider how such stark spectral and photophysical changes are related to the DNA structure and silver stoichiometry. First, the sensor changes from a folded, single-stranded precursor to a dimeric, hybridized duplex, as shown by using Na^+ and oligonucleotide concentrations to alter reaction progress and by using fluorescence anisotropy, fluorescence correlation spectroscopy, and size exclusion chromatography to establish structures. These alternate polymorphic forms of DNA arise through interactions with their respective silver cluster ligands. Second, the net amount of bound silver doubles when the precursor strand converts to its dimeric hybrid, as shown by atomic emission studies of purified conjugates. These two observations emphasize how DNA-bound clusters act both as reporters of their DNA environment and as ligands that alter DNA structure.

Experimental

Materials

Silver nitrate (Acros) and sodium borohydride (Aldrich) were used as received. The following oligonucleotides (Integrated DNA Technologies) were received as lyophilized, desalted samples with no further purification: $C_3AC_3AC_3TC_3A$-CCCGCCGCTGGA (T3-S_A), $C_3AC_3AC_3TC_3A$-TT-CCCGCCGCTGGA (T3-T_2-S_A), $C_3AC_3AC_3TC_3A$-TTTTTT-CCCGCCGCTGGA (T3-T_6-S_A), TCCAGCGGCGGG (S_{Ac}), $C_3AC_3AC_3TC_3A$-TT-CCCGCC (T3-T_2-S_B), GCGGCGGG (S_{Bc}), $C_3AC_3AC_3TC_3A$-TCAACATCAGTCTGATAAGCTA (T3-S_C), and TAGCTTATCAGACTGATGTTGA (S_{Cc}), where the strand polarity is $5' \rightarrow 3'$, T3 is a template for a near-infrared cluster and refers to the substitution of adenine with thymine in the third C_3X motif, S_A and S_C are recognition sites derived from the genome of bacteriophage lambda and from the 22-base recognition element for a cancer related microRNA, respectively, S_B is a truncated variant of S_A, and S_{Ac}, S_{Bc}, and S_{Cc} are the complements to S_A, S_B, and S_C, respectively.[18,27,44,45] In relation to our earlier studies, the two base extension of S_{Bc} relative to the recognition site S_C does not influence the cluster transformation.[18] The 12 base pair duplex S_A:S_{Ac} was used in most of these studies because it is stable in lower ionic strength buffers, as indicated by its melting temperature of 64 °C when using 30 μM oligonucleotides in a solution with 26 mM Na^+.[46] Following hydration, the concentration of these solutions were measured using the

absorbance at 260 nm based on extinction coefficients derived from the nearest-neighbor approximation, and an 8% hypochomicity associated with base stacking in the duplex portion S_A:S_{Ac} was accounted for in the calculation.[47] Concentrations were derived using a pH = 9.8 borate/boric acid buffer, which disrupts aggregates favored by cytosine-rich strands.[48,49]

Synthesis

The precursor silver conjugate was formed by first combining 8 equivalents of Ag^+:oligonucleotide with a 90 μM solution of oligonucleotide in a 10 mM citrate/citric acid buffer at pH = 6.5, which gives a $[Na^+] \approx 26$ mM.[50] This solution was heated at 80 °C for 5 mins to disrupt DNA aggregates and then cooled prior to reduction with 4 equivalents of BH_4^-:oligonucleotide. Prior studies indicate that this relative amount has a minor impact on the synthetic outcome.[18] This solution was immediately transferred to a high pressure vessel with 500 psi O_2 at room temperature, and after >3 hrs, the sample was diluted three-fold in a buffer supplemented with $NaClO_4$ to yield a solution with 30 μM oligonucleotide. After adding the complement, the sample was heated to 50 °C for 20 mins and then cooled to room temperature for characterization.

Characterization

Absorption spectra were acquired with a Cary 50 (Varian) at a scan rate of 600 nm/min using an appropriate buffer baseline and using plastic cuvettes that are transparent to UV and visible light (BrandTech). Emission spectra were acquired with a FluoroMax-3 (Jobin Yvon) using quartz cells at a scan rate of 2 nm/s and 0.5 s integration, and variations in the lamp intensity were corrected using a reference detector. Size exclusion chromatography was conducted with a Shimadzu Prominence high performance liquid chromatography system using a 300 × 7.8 mm BioSep-SEC-S2000 column (Phenomenex), having 5 μm particles and a pore size of 145 Å. The mobile phase was buffered at pH = 6.5 with 10 mM citrate/citric acid that was supplemented with $NaClO_4$ to minimize solute interactions with the stationary phase.[51] To assess hydrodynamic radii, size standards were based on the thymine oligonucleotides dT_{10}, dT_{15}, dT_{20}, and dT_{30}.[13,52] For sample isolation, timing between spectral identification using the absorption spectrometer (SPD-M20A) and the fraction collection (FRC-10A) was determined using a concentrated solution of dye. Subsequently, a consecutive series of samples was collected from an injection of a DNA solution, and the time adjusted chromatogram matched the absorbances at 260 nm in the collected fractions. To eliminate a preceding DNA species form the desired single-stranded conjugate with the violet-absorbing cluster, Gaussian fitting was used to temporally resolve the species (Figure S3A and S3B). The repeatability of the retention times allowed specific isolation of the desired cluster conjugate. The large size of near-infrared conjugate allowed its isolation from competing species (Figure S3D and S3E). For both types of clusters, correspondence between the retention time derived from the DNA absorbance at 260 nm and the cluster absorbances at 400 nm and 730 nm indicates that no competing species contaminate the isolated fractions (Fig. S3C and S3D). Following collection, the samples were analyzed using an inductively coupled plasma – optical emission spectrometer (Optima 7300 DV, Perkin Elmer). Nitric acid was added to a final concentration of 10% (v/v), and a yttrium reference with emission at 371.03 nm was added to account for variations in the

sample delivery rate. Silver and phosphorus standards (High Purity Standards) were used to generate calibration curves, and control samples containing oligonucleotide and Ag^+ were used to account for matrix effects.[27] A peristaltic pump delivered the samples to the nebulizer and the argon plasma. To relate the phosphorus and oligonucleotide concentrations, the lengths were derived from the DNA sequences, after accounting for the absence of the 3′ terminal phosphate. Silver and phosphorus were detected using their emissions at 328.07 and 214.91 nm, respectively, and the optical chamber was purged with nitrogen to detect the UV emission from phosphorus. Fluorescence anisotropies were derived using

$$r = \frac{I_{VV} - GI_{VH}}{I_{VV} + 2GI_{VH}}$$

where I_{VV} and I_{VH} are the vertically and horizontally polarized emissions, respectively, using vertically polarized excitation and G is the sensitivity factor that describes the response of the detection system to vertically and horizontally polarized light.[6,53] Ten background-corrected intensity measurements were used. The anisotropy of the duplex sensor was measured using the dimeric cyanine dye YOYO-1 (Invitrogen), which has a high affinity for duplex DNA.[54,55] As in an earlier studies, fluorescence correlation spectroscopy was conducted using diode laser excitation at 690 nm, and cluster concentrations were derived using a solution of Cy7 to calibrate the probe volume.[30]

Results

The sensor has two general components (Fig. 1). We chose the sequence CCCGCCGCTGGA (abbreviated S_A) for the 3′ region because it forms a stable duplex with its target complement over a range of salt and oligonucleotide concentrations. However, recognition sites are interchangeable, as demonstrated by sensors with S_B and S_C that exhibit similar spectral changes (Fig. S1).[18] We chose $C_3AC_3AC_3TC_3A$ (abbreviated T3) as the leading 5′ sequence because it is a template for an ~10 silver atom cluster with strong near infrared absorption and emission.[27] The composite strand acts as a sensor because two spectroscopically-distinct silver clusters interconvert when a target associates with the recognition site, as signaled by a shift in absorption from 400 to 730 nm and recovery of 790 nm emission (Fig. 1). Our studies show that these spectral and photophysical changes emanate from changes in both DNA structure and the amount of bound silver.

Sensor Design

One factor underlying the analyte response is the structure of the sensor. This contribution was first explored by modulating coupling between the two sensor components. Three sensors with thymine spacers (bolded) between the cluster template (T3) and recognition site (S_A) are evaluated: $C_3AC_3AC_3TC_3A$-CCCGCCGCTGGA (T3-S_A), $C_3AC_3AC_3TC_3A$-**TT**-CCCGCCGCTGGA (T3-T_2-S_A), and $C_3AC_3AC_3TC_3A$-**TTTTTT**-CCCGCCGCTGGA (T3-T_6-S_A) (Fig. 2). Thymine was chosen because it does not support emissive silver species at neutral pH and because it's flexibility facilitates DNA folding.[6,56] Resulting DNA

environments for both violet and near infrared clusters were monitored by absorption spectroscopy. The violet absorbing cluster is selectively generated by controlling three factors: stoichiometries $\lesssim$10 Ag^+:oligonucleotide limit agglomeration, oxygen eliminates competing species possibly through oxidative etching, and low ionic strength disfavors alternate clusters that form aggregated DNA hosts (Figs. 2 and S2).[18,57] All three sensors have similar λ_{max} values, which suggest that thymine modifications are inherently innocuous. However, the number of intervening thymines direct the amount of cluster produced and its extent of conversion, which suggests that the cluster environment is defined by the relative positions of the 5′ and 3′ sensor components. Based on the high absorbance at 400 nm and its near extinction due to hybridization, the TT-linked sensor (T3-T_2-S_A) was chosen for subsequent studies. A favored 1 target:sensor stoichiometry shows that hybridization drives this transformation, but a tempered response over the range of target concentrations suggests that target binding is inhibited (Fig. S4).

Sensor Opening and Aggregation

Large-scale DNA reorganization accompanies the spectral changes of the associated clusters. The violet and near infrared clusters that track the analyte response were monitored using their spectroscopic signatures. The structures of their associated DNA hosts were evaluated by size exclusion chromatography. Native single-stranded T3-T_2-S_A and duplex T3-T_2-S_A:S_{Ac} were used as references. Structural perturbation is first evident for the precursor T3-T_2-S_A, whose association with the violet-absorbing cluster produces a longer retention time and a 30% smaller hydrodynamic radius (Fig. 3A:a′→a). This conjugate elutes earlier with addition of the complement (Fig. 3A:a → 3B:b), and a parallel shift for the native sensor supports duplex formation in both cases (Fig. 3A:a′ → 3B:b′). However, this new duplex-cluster conjugate mimics its precursor because it retains a violet absorption band (Figure 3C:a→b) and it is folded relative to its native host T3-T_2-S_A:S_{Ac} (Fig. 3B:b′→b). Thus, this preservation of the electronic and structural environment for the violet absorbing cluster demonstrates that target recognition through hybridization is not solely responsible for formation of the near infrared cluster.

Salt triggers the requisite structural change that guides cluster transformation (Fig. 3C:b→c). Supplementing the 10 mM citric acid/citrate buffer with 300 mM $NaClO_4$ produces an even shorter retention time for the resulting near infrared conjugate, thus supporting an aggregated DNA motif in relation to the native duplex T3-T_2-S_A:S_{Ac} (Fig. 3B:b→c). This reaction is inhibited in reverse order when the salt concentration is increased first without the complement (Fig. S5a). Similar spectral responses with $NaClO_4$ and $NaNO_3$ indicate that Na^+ electrostatically stabilizes the DNA host (Fig. S5b). [58] The conversion is restrained by reducing the oligonucleotide concentration 100-fold from 30 to 0.3 μM, which indicates intermolecular strand association in the duplex sensors (Fig. S5c).

Fluorescence anisotropy, fluorescence correlation spectroscopy, and size exclusion chromatography measurements establish the aggregate structure. A fluorescence anisotropy of 0.31 ± 0.01 for the near infrared emitting silver cluster conjugate is interpreted using two references. First, the organic fluorophore Cy7 (λ_{ex} = 750 nm/λ_{em} = 790 nm) in glycerol has an anisotropy of 0.38 ± 0.01, and similarly large values suggests that a large DNA matrix

constrains the near infrared cluster while the viscous solvent limits mobility for the organic dye. Second, a fluorescence anisotropy of native T3-T_2-S_A:S_{Ac} was measured using YOYO-1 that intercalates with the duplex S_A:S_{Ac} portion.[54] This strongly associating dye only emits when bound to DNA and is thus expected to fluorescently track the global motions of its DNA host. A low concentration of 1 dye:sensor limits DNA structural changes.[55] A relatively small fluorescence anisotropy of 0.11 ± 0.01 is expected for a small oligonucleotide and provides further support for the large size for the near infrared conjugate.[6,59,60]

The cluster:strand stoichiometry is deduced from the absorption spectra of purified conjugates. The contributions of each chromophore to the observed absorbances is evaluated from their respective extinction coefficients. The extinction coefficient of the near infrared cluster is 270,000 ± 30,000 M^{-1} cm^{-1} at 730 nm, based on concentrations derived from fluorescence correlation spectroscopy (Fig. S6). The extinction coefficient of native T3-T_2-S_A:S_{Ac} is 335,600 $M^{-1}cm^{-1}$ at 260 nm, based on nearest neighbor coupling between the nucleobases and hypochromicity associated with the duplex. The λ_{max} for this band is not altered in the cluster complex, so relative amounts of DNA and cluster are inferred from the independent absorbances of these two chromophores. Using five separately prepared and chromatographically resolved samples, the relative absorbance is 2.4 ± 0.2 for the electronic transitions at 260 and 730 nm, respectively. This matches a ratio of extinction coefficients of 2.5 derived using one cluster associated with two hybridized sensors (Figures 4C).

Modified complements further substantiate sensor dimerization. A dT_{10} tail on the 5′ terminus of the target sequence distinguishes the hybridized complex by its larger hydrodynamic radius (Fig. 4A). This appendage is removed from the cluster binding site because the complement forms an antiparallel duplex with the recognition site. As with its unmodified counterpart, this larger complement generates the same near infrared conjugate only with earlier elution. These modified and unmodified targets were mixed in equal proportions, and a distinctive triplet pattern emerged (Fig. 4B). The outer peaks have retention times that match the two control samples, thus indicating that the central peak arises from an aggregate incorporating both complements. Relative absorbances follow a 1.1: 2.0: 1.0 pattern, which is similar to a statistical weighting expected of a dimer with two equivalent binding sites. The species associated with the central peak was isolated and subsequently heated to reestablish the triplet pattern, which supports noncovalent assembly in the aggregate (Fig. S7). Cluster development as high as pH = 10 suggests that interstrand linkage is not strongly dependent on base protonation (Fig. S8).[61]

Silver Stoichiometry

A second factor contributing the analyte response is large-scale reorganization of bound silver. Relative silver:DNA stoichiometries were determined using atomic emission from silver and the surrogate phosphorous, respectively.[3,8,62] This analysis used spectrally and chemical pure complexes that were isolated based on their distinctive structures by size exclusion chromatography. The folded precursor sensor harbors 11.1 ± 1.1 Ag/T3–T_2–S_A, and alternate templates that are 2 bases shorter (T3-S_A) and 8 bases longer (T3-S_C) have 11.0 ± 1.1 Ag: and 10.7 ± 1.0 Ag:oligonucleotide, respectively. These similar silver

stoichiometries are higher relative to earlier studies that used absorption spectroscopy to measure oligonucleotide concentrations, and the discrepancy may be attributed to cluster-induced folding that alters nucleobase conformations and their extinction coefficients.[18,47] Atomic emission studies that measure both silver and phosphorus concentrations are expected to be more reliable, and two further variations were considered. First, a mobile phase with a lower concentration of 40 mM $NaClO_4$ also effectively separated the complex, and 10.9 ± 1.0 Ag/T3-T_2-S_A was again derived through atomic emission. Second, reversed-phase separation using a binary gradient of methanol and 50 mM triethylamine acetate isolated a complex with 11.2 ± 0.9 Ag/T3-T_2-S_A. Similarities across different oligonucleotides and alternate separation conditions indicate that the cluster has ~11 silver atoms. This preferred stoichiometry is also reflected in the initial Ag^+ concentrations (Fig. S2). Up to 10 Ag^+, only a single optical transition with λmax = 400 nm is observed, and its increasing absorbance at a constant λmax is consistent with cluster development in a particular binding site. At higher stoichiometries, cluster growth is no longer constrained, and alternate species develop with longer wavelength absorptions.

Chromatographically-purified, hybridized near infrared conjugates have 11.5 ± 1.2 Ag/T3–T_2–S_A:S_{Ac} and 11.7 ± 1.1 Ag/T3–S_A:S_{Ac}, consistent with previous results (Fig. S3D).[18] These empirical stoichiometries are similar to the ~11 silver atoms associated with their respective predecessors, and this consistency through hybridization suggests that a favored binding site within the $C_3AC_3AC_3TC_3A$ sequence is conserved. Because fluorescence anisotropy, fluorescence correlation spectroscopy, and size exclusion chromatography studies support a dimeric hybridized sensor host for the near infrared cluster, the net stoichiometries are 23.0 ± 1.7 Ag:(T3-T_2-S_A:S_{Ac})$_2$ and 23.4 ± 1.6 Ag:(T3-S_A:S_{Ac})$_2$. Recent mass spectral studies have also identified cluster-DNA conjugates with similar amounts of silver.[63]

Discussion

A 330 nm red-shift in absorption and a background-limited enhancement in near infrared emission occurs when a silver cluster-DNA conjugate hybridizes with its complementary target. One factor associated with this spectral and photophysical switching is unfolding and dimerization of the sensor strand. Analogously, conformational changes are the linchpin of molecular beacons, in which target oligonucleotides open the sensor and sever coupling between terminally-labeled organic dyes.[64] Silver clusters are distinctive chromophores because they not only signal but also direct their DNA environments. An ~11 atom cluster that associates with T3-T_2-S_A distinguishes this precursor sensor through its condensation relative to the native conformation as well as its associated violet absorption. Folding may be driven by electrostatic neutralization of the phosphate backbone, as the oxidizing agents O_2 and H_2O_2 used to produce this cluster may yield a cationic species.[18] Prior studies have established the stability of such cations and their propensity to form crosslinks within biopolymer substrates.[13,14,65] Additionally, intrastrand condensation may emanate from nucleobase coordination. Ag^+ favors linear coordination complexes with nucleobases, and silver clusters may interact similarly with multiple nucleobases within a strand, as suggested by cluster effects on the sizes and electrophoretic mobilities of their DNA hosts.[13,14,66] Beyond the innate impact of a metallic ligand, folding is also guided by strand

modifications. Two implications are considered from the effects of adjoining thymines between the cluster template and analyte recognition moieties (Fig. 2). First, the number of intervening thymines determines how the cluster forms and transforms, and we are interested in understanding whether concepts that explain DNA hairpin folding might be applicable to silver cluster conjugates.[67] Second, strand association with the cluster-laden sensor is mildly inhibited, so cluster-induced folding may sequester the recognition site in the sensor (Fig. S4). We are interested in understanding how noncanonical metal-nucleobase interactions could be utilized to distinguish closely related analytes.[66,68–71]

Global constraint imposed by the violet cluster is relieved by hybridization. Beyond simply opening, the hybridized sensors dimerize to create two equivalent target recognition sites, and this higher-order DNA assembly now features near infrared absorption and emission (Fig. 4). Self-association originates through $C_3AC_3AC_3TC_3A$, as suggested by sensors with alternate recognition sites that yield similar spectral changes (Fig. S1). One possible structural arrangement is a four-stranded, i-motif, which is favored by such cytosine-rich sequences when the solution pH is similar to the pK_a of cytosine (4.5).[47,61] However, alternate models are needed for the cluster conjugates because only two sensors assemble and cluster transformation is robust at high pH where cytosine N3 protonation is strongly disfavored (Fig. S8).[48] These observations suggest that the near infrared cluster drives DNA structural change, a characteristic shared with its violet absorbing precursor. Two possibilities with parallel and antiparallel arrangements are considered in Figure 4C, and these might be distinguished via steric interactions between larger thymine appendages on the complements. Recent studies have identified dimeric strand-cluster conjugates by electrospray ionization mass spectrometry.[63] While droplet evaporation might promote strand association through solute concentration, our studies indicate that such species are stable in dilute solution conditions.

A second factor contributing to the cluster transformation is a two-fold increase in the amount of bound silver. This assessment is based on chromatographically isolating chemically and spectrally pure conjugates followed by elemental analysis to determine the relative amounts of silver and DNA.[2,4,72,73] Empirical stoichiometries are conserved with both T3-T_2-S_A and T3-T_2-S_A:S_{Ac} binding ~11 Ag. However, the latter hybrid forms a dimer (T3-T_2-S_A:S_{Ac})$_2$ and thus hosts twice the amount of silver. Similar empirical stoichiometries suggest that two violet-absorbing clusters assemble to produce near infrared absorption and emission (Fig. 4D). Resulting cluster segregation or coalescence is considered based on studies with $C_3AC_3AC_3TC_3A$ (T3).[27] Both (T3-T_2-S_A:S_{Ac})$_2$ and the abstracted T3 provide analogous electronic and chemical environments for clusters with similar near infrared spectra. Additionally, the two hosts have comparable empirical amounts of silver when measurement uncertainties are considered, as 9.6 ± 0.8 Ag atom complex with $C_3AC_3AC_3TC_3A$. However, T3 and (T3-T_2-S_A:S_{Ac})$_2$ are distinguished by their monomeric and dimeric strand stoichiometries, respectively. Thus, similar empirical silver stoichiometries but differing strand compositions suggests that two distinct clusters within (T3-T_2-S_A:S_{Ac})$_2$ mimic the single cluster bound to monomeric T3 (Fig. 4D). Proximal clusters in (T3-T_2-S_A:S_{Ac})$_2$ could have altered spectral properties due to electronic coupling, as suggested by a measured extinction coefficient of 272, 000 $M^{-1}cm^{-1}$ that is less than twice the value of 180,000 $M^{-1}cm^{-1}$ for the T3-bound cluster. Further evidence of

electronic perturbation are the shifts in the absorption maxima from 750 nm to 730 nm and emission maxima from 810 to 790 nm when comparing T3 and $(T3\text{-}T_2\text{-}S_A{:}S_{Ac})_2$, respectively. This model for silver organization suggests that nucleobase coordination restrains metal agglomeration, and we are working to address this question by modifying the sequence of the cluster template.[24] Higher resolution studies using mass spectrometry may provide important insight into the cluster changes.[63]

Conclusion

These studies consider a hybrid sensor in which silver clusters are conjugated with DNA strands. The key observation is that high contrast spectral and photophysical changes accompany association of analyte strands with the cluster-laden sensor. These changes occur because these metallic ligands alter the shape and structure of their DNA hosts and because the organization of bound silver changes. The extent to which these concepts apply to other types of DNA-bound silver clusters may provide an avenue understanding their analyte signaling capabilities.

Supplementary Material

Refer to Web version on PubMed Central for supplementary material.

Acknowledgments

We thank the National Science Foundation (CBET-0853692) and Henry Dreyfus Teacher-Scholar Awards Program for support of this work. We are grateful to the National Institutes of Health (R15GM071370) and National Science Foundation (CHE-0922834) for primary support during the initial stages of this work. In addition, we thank the National Science Foundation (CHE-0718588 and CHE-0922834). I.M., D.N., and O.S. were supported by undergraduate research fellowships provided through the Regional NSF-REU Site in Chemistry at Furman University, the Furman Advantage program, and a USE Award to Furman University from the Howard Hughes Medical Institute, respectively. J.P. is grateful for the support provided by the Henry Keith and Ellen Hard Townes Professorship.

References

1. Wilcoxon JP, Abrams BL. Chem Soc Rev. 2006; 35:1162–1194. [PubMed: 17057844]
2. Parker JF, Fields-Zinna CA, Murray RW. Acc Chem Res. 2010; 43:1289–1296. [PubMed: 20597498]
3. Zheng J, Nicovich PR, Dickson RM. Annu Rev Phys Chem. 2007; 58:409. [PubMed: 17105412]
4. Petty JT, Zheng J, Hud NV, Dickson RM. J Am Chem Soc. 2004; 126:5207–5212. [PubMed: 15099104]
5. Ritchie CM, Johnsen KR, Kiser JR, Antoku Y, Dickson RM, Petty JT. J Phys Chem C. 2007; 111:175–181.
6. Sengupta B, Ritchie CM, Buckman JG, Johnsen KR, Goodwin PM, Petty JT. J Phys Chem C. 2008; 112:18776–18782.
7. Neidig ML, Sharma J, Yeh HC, Martinez JS, Conradson SD, Shreve AP. J Am Chem Soc. 2011; 133:11837–11839. [PubMed: 21770404]
8. Soto-Verdugo V, Metiu H, Gwinn E. J Chem Phys. 2010; 132:195102. [PubMed: 20499990]
9. O'Neill PR, Gwinn EG, Fygenson DK. J Phys Chem C. 2011; 115:24061–24066.
10. Gwinn EG, O'Neill P, Guerrero AJ, Bouwmeester D, Fygenson DK. Adv Mater. 2008; 20:279–283.

11. Richards CI, Choi S, Hsiang JC, Antoku Y, Vosch T, Bongiorno A, Tzeng YL, Dickson RM. J Am Chem Soc. 2008; 130:5038–5039. [PubMed: 18345630]
12. Sharma J, Yeh HC, Yoo H, Werner JH, Martinez JS. Chem Commun. 2010; 46:3280–3282.
13. Sengupta B, Springer K, Buckman JG, Story SP, Abe OH, Hasan ZW, Prudowsky ZD, Rudisill SE, Degtyareva NN, Petty JT. J Phys Chem C. 2009; 113:19518–19524.
14. Driehorst T, O'Neill P, Goodwin PM, Pennathur S, Fygenson DK. Langmuir. 2011; 27:8923–8933. [PubMed: 21682258]
15. Yang SW, Vosch T. Anal Chem. 2011; 83:6935–6939. [PubMed: 21859161]
16. Latorre A, Somoza Á. Chembiochem. 2012; 13:951–958. [PubMed: 22508551]
17. Han BY, Wang EK. Analytical and Bioanalytical Chemistry. 2012; 402:129–138. [PubMed: 21858647]
18. Petty JT, Story SP, Juarez S, Votto SS, Herbst AG, Degtyareva NN, Sengupta B. Anal Chem. 2012; 84:356–364. [PubMed: 22098274]
19. Shah P, Rorvig-Lund A, Ben Chaabane S, Thulstrup PW, Kjaergaard HG, Fron E, Hofkens J, Yang SW, Vosch T. ACS Nano. 2012; 6:8803–8814. [PubMed: 22947065]
20. Lavis LD, Raines RT. ACS Chem Biol. 2008; 3:142–155. [PubMed: 18355003]
21. Vosch T, Antoku Y, Hsiang JC, Richards CI, Gonzalez JI, Dickson RM. Proc Natl Acad Sci U S A. 2007; 104:12616–12621. [PubMed: 17519337]
22. Patel SA, Cozzuol M, Hales JM, Richards CI, Sartin M, Hsiang JC, Vosch T, Perry JW, Dickson RM. J Phys Chem C. 2009; 113:20264–20270.
23. Richards CI, Hsiang JC, Senapati D, Patel S, Yu J, Vosch T, Dickson RM. J Am Chem Soc. 2009; 131:4619–4621. [PubMed: 19284790]
24. Petty JT, Fan C, Story SP, Sengupta B, Sartin M, Hsiang JC, Perry JW, Dickson RM. J Phys Chem B. 2011; 115:7996–8003. [PubMed: 21568292]
25. Pauli J, Vag T, Haag R, Spieles M, Wenzel M, Kaiser WA, Resch-Genger U, Hilger I. Eur J Med Chem. 2009; 44:3496–3503. [PubMed: 19269067]
26. Allen PM, Liu W, Chauhan VP, Lee J, Ting AY, Fukumura D, Jain RK, Bawendi MG. J Am Chem Soc. 2010; 132:470–471. [PubMed: 20025222]
27. Petty JT, Fan C, Story SP, Sengupta B, St John Iyer A, Prudowsky Z, Dickson RM. J Phys Chem Lett. 2010; 1:2524–2529. [PubMed: 21116486]
28. Chance B. Ann N Y Acad Sci. 1998; 838:29–45. [PubMed: 9511793]
29. Frangioni JV. Curr Opin Chem Biol. 2003; 7:626–634. [PubMed: 14580568]
30. Petty JT, Sengupta B, Story SP, Degtyareva NN. Anal Chem. 2011; 83:5957–5964. [PubMed: 21702495]
31. Li J, Zhong X, Zhang H, Le XC, Zhu JJ. Anal Chem. 2012; 84:5170–5174. [PubMed: 22607314]
32. Chen WY, Lan GY, Chang HT. Anal Chem. 2011; 83:9450–9455. [PubMed: 22029551]
33. Ntziachristos V, Bremer C, Weissleder R. European Radiology. 2003; 13:195–208. [PubMed: 12541130]
34. Guo W, Yuan J, Dong Q, Wang E. J Am Chem Soc. 2010; 132:932–934. [PubMed: 20038102]
35. Guo W, Yuan J, Wang E. Chem Commun. 2011; 47:10930–10932.
36. Lan GY, Chen WY, Chang HT. Biosens Bioelectron. 2011; 26:2431–2435. [PubMed: 21074985]
37. Sharma J, Yeh HC, Yoo H, Werner JH, Martinez JS. Chem Commun. 2011; 47:2294–2296.
38. Li J, Zhong X, Cheng F, Zhang JR, Jiang LP, Zhu JJ. Anal Chem. 2012; 84:4140–4146. [PubMed: 22482827]
39. Guo W, Yuan J, Wang E. Chem Commun. 2009; 23:3395–3397.
40. Su YT, Lan GY, Chen WY, Chang HT. Anal Chem. 2010; 82:8566–8572. [PubMed: 20873802]
41. Hsin-Chih Y, Sharma J, Han JJ, Martinez JS, Werner JH. Nanotechnology Magazine, IEEE. 2011; 5:28–33.
42. Yeh HC, Sharma J, Shih IM, Vu DM, Martinez JS, Werner JH. J Am Chem Soc. 2012; 134:11550–11558. [PubMed: 22775452]
43. Yeh HC, Sharma J, Han JJ, Martinez JS, Werner JH. Nano Lett. 2010; 10:3106–3110. [PubMed: 20698624]

44. Nichols BP, Donelson JE. J Virol. 1978; 26:429–434. [PubMed: 666898]
45. Li J, Schachermeyer S, Wang Y, Yin Y, Zhong W. Anal Chem. 2009; 81:9723–9729. [PubMed: 19831385]
46. Owczarzy R, Tataurov AV, Wu Y, Manthey JA, McQuisten KA, Almabrazi HG, Pedersen KF, Lin Y, Garretson J, McEntaggart NO, Sailor CA, Dawson RB, Peek AS. Nucleic Acids Res. 2008; 36:W163–W169. [PubMed: 18440976]
47. Bloomfield, VA.; Crothers, DM.; Tinoco, J.; Ignacio. Nucleic Acids: Structures, Properties, and Functions. University Science Books; Sausaltio, CA: 2000.
48. Brown DM, Gray DM, Patrick MH, Ratliff RL. Biochemistry. 1985; 24:1676–1683. [PubMed: 4005222]
49. Gueron M, Leroy JL. Current Opinion in Structural Biology. 2000; 10:326–331. [PubMed: 10851195]
50. Goldberg RN, Kishore N, Lennen RM. J Phys Chem Ref Data. 2002; 31:231–370.
51. Leroy JL, Gehring K, Kettani A, Gueron M. Biochemistry. 1993; 32:6019–6031. [PubMed: 8389586]
52. Doose S, Barsch H, Sauer M. Biophys J. 2007; 93:1224–1234. [PubMed: 17513377]
53. Lakowicz, JR. Principles of Fluorescence Spectroscopy. 3. Springer; New York: 2006.
54. Rye HS, Yue S, Wemmer DE, Quesada MA, Haugland RP, Mathies RA, Glazer AN. Nucleic Acids Res. 1992; 20:2803–2812. [PubMed: 1614866]
55. Bordelon JA, Feierabend KJ, Siddiqui SA, Wright LL, Petty JT. J Phys Chem B. 2002; 106:4838–4843.
56. Vallone PM, Paner TM, Hilario J, Lane MJ, Faldasz BD, Benight AS. Biopolymers. 1999; 50:425–442. [PubMed: 10423551]
57. Ivanova OS, Zamborini FP. J Am Chem Soc. 2010; 132:70–72. [PubMed: 20000318]
58. Manning GS. Q Rev Biophys. 1978; 11:179–246. [PubMed: 353876]
59. Nakamura M, Fukunaga Y, Sasa K, Ohtoshi Y, Kanaori K, Hayashi H, Nakano H, Yamana K. Nucleic Acids Res. 2005; 33:5887–5895. [PubMed: 16237124]
60. Juskowiak B, Galezowska E, Zawadzka A, Gluszynska A, Takenaka S. Spectrochimica Acta Part A: Molecular and Biomolecular Spectroscopy. 2006; 64:835–843.
61. Phan AT, Gueron M, Leroy JL. Methods Enzymol. 2001; 338:341–371. [PubMed: 11460557]
62. Bonacic-Koutecky V, Veyret V, Mitric R. J Chem Phys. 2001; 115:10450–10460.
63. Schultz D, Gwinn EG. Chem Commun. 2012; 48:5748–5750.
64. Tyagi S, Kramer FR. Nat Biotechnol. 1996; 14:303–308. [PubMed: 9630890]
65. Kulesza A, Mitrić R, Bonačić-Koutecký V, Bellina B, Compagnon I, Broyer M, Antoine R, Dugourd P. Angew Chem Int Ed. 2011; 50:878–881.
66. Lippert B. Coord Chem Rev. 2000; 200–202:487–516.
67. Varani G. Annu Rev Biophys Biomolec Struct. 1995; 24:379–404.
68. Müller J. European Journal of Inorganic Chemistry. 2008; 2008:3749–3763.
69. Miyake Y, Togashi H, Tashiro M, Yamaguchi H, Oda S, Kudo M, Tanaka Y, Kondo Y, Sawa R, Fujimoto T, Machinami T, Ono A. J Am Chem Soc. 2006; 128:2172–2173. [PubMed: 16478145]
70. Wang Y, Li J, Wang H, Jin J, Liu J, Wang K, Tan W, Yang R. Anal Chem. 2010; 82:6607–6612. [PubMed: 20597497]
71. Tsourkas A, Behlke MA, Rose SD, Bao G. Nucleic Acids Res. 2003; 31:1319–1330. [PubMed: 12582252]
72. Guo J, Kumar S, Bolan M, Desireddy A, Bigioni TP, Griffith WP. Anal Chem. 2012; 84:5304–5308. [PubMed: 22594913]
73. O'Neill PR, Velazquez LR, Dunn DG, Gwinn EG, Fygenson DK. J Phys Chem C. 2009; 113:4229–4233.

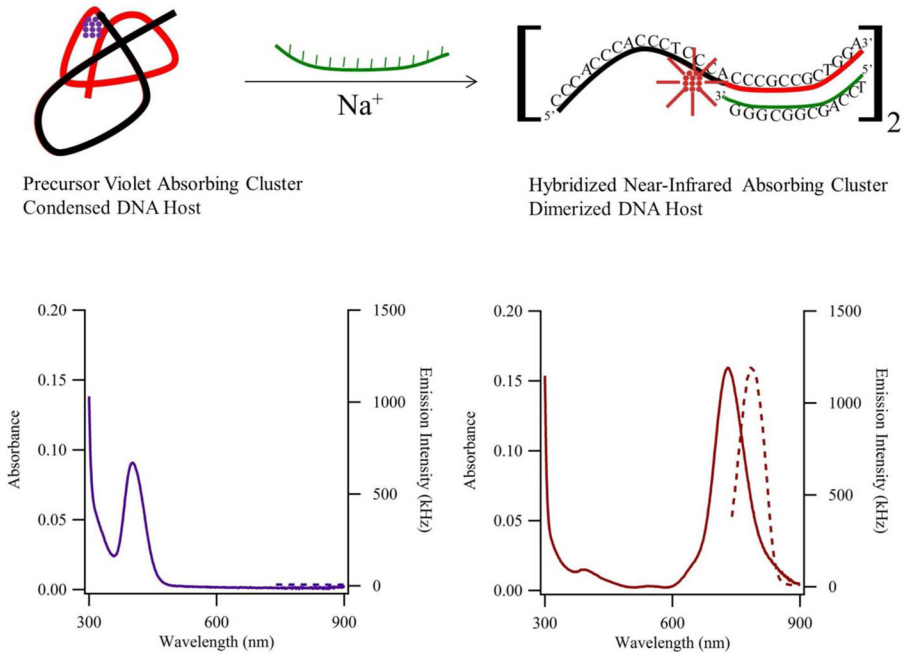

Figure 1.

The reaction summarizes how the structure of the sensor strand and the stoichiometry of the cluster are linked with the changes in the absorption (solid lines – left axes) and emission (dotted lines – right axes) spectra in the lower panels. (Left) The sensor is comprised of a cluster template (black portion=$C_3AC_3AC_3TC_3A$) and a recognition site (red portion=CCCGCCGCTGGA) and is folded by an ~11 silver atom cluster (violet) with λ_{max} = 400 nm and undetectable near infrared emission. (Right) Addition of the complementary strand (green) with salt opens the sensor strand with ensuing dimerization via cluster crosslinking. The absorption of the resulting cluster red-shifts to 730 nm, and high-contrast detection is also accomplished by a background-limited enhancement of the near infrared emission. The relative silver stoichiometry is conserved, thereby doubling the net amount of bound silver in the aggregated sensor.

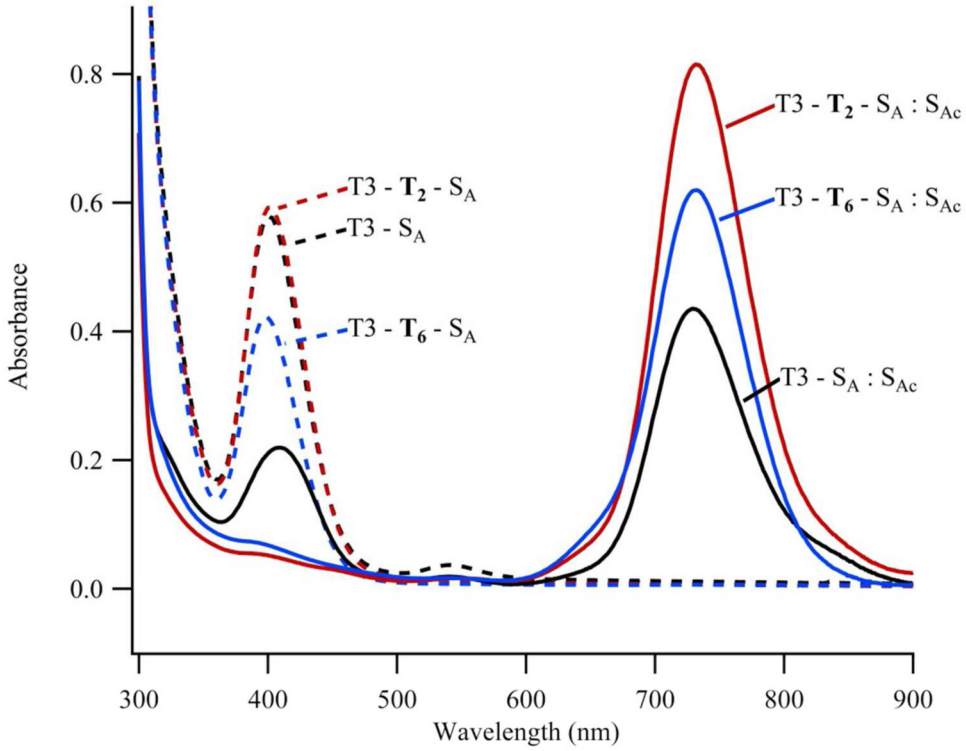

Figure 2.

Linkage between the cluster template and the recognition site was controlled by varying the length of thymine spacers in three sensor strands: T3–S_A (black), T3–T_2–S_A (red), and T3–T_6–S_A (blue). The violet-absorbing precursor forms and has similar absorption maxima with all three strands, indicating that this cluster is supported in similar electronic environments (dotted lines). After adding the complement, all three sensors support conversion to the near-infrared cluster (solid lines). Based on high cluster absorbance at 400 nm and large spectral contrast associated with the complement, T3–T_2–S_A was chosen for subsequent studies.

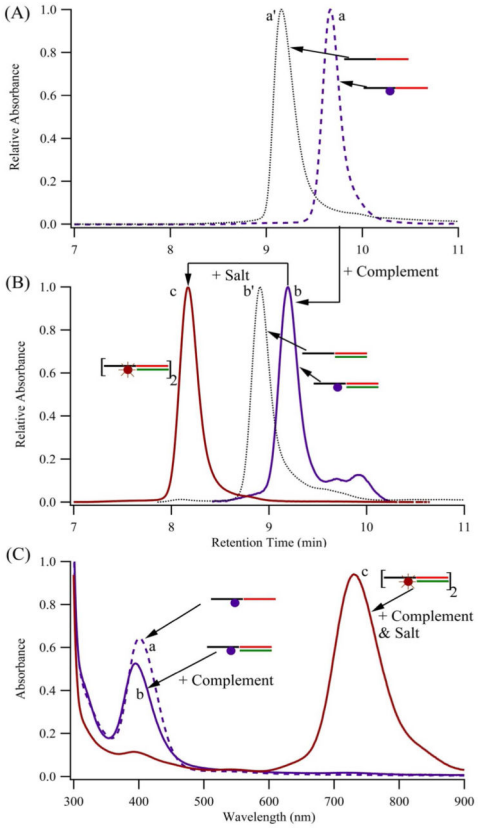

Figure 3.

Size exclusion chromatography shows that development of the near infrared cluster depends on hybridization between the recognition site of the sensor and its complement and on the concentration of Na^+. Chromatograms were acquired for T3–T_2–S_A alone (A:a′-black dotted line), its conjugate with the violet-absorbing cluster (A:a-dashed violet line), the monomeric duplex T3-T_2-S_A:S_{Ac} alone (B:b′-dotted black line), and its monomeric conjugate with the violet-absorbing cluster (B:b-solid violet line) that were prepared in low ionic strength 10 mM citrate/citric acid buffer. In relation to their single-stranded analogs, these hybridized analogs have shortened retention times that support formation of the duplex with the recognition site. The violet absorption is retained through duplex formation (C:a→b), and both T3-T_2-S_A and T3-T_2-S_A:S_{Ac} are condensed by the violet absorbing cluster in relation to their native forms (A:a→a′ and B:b→b′). The near-infrared cluster (B:c and C:c-solid dark red line) develops when salt is added, and the still earlier elution of this conjugate supports its large size in relation to the duplex.

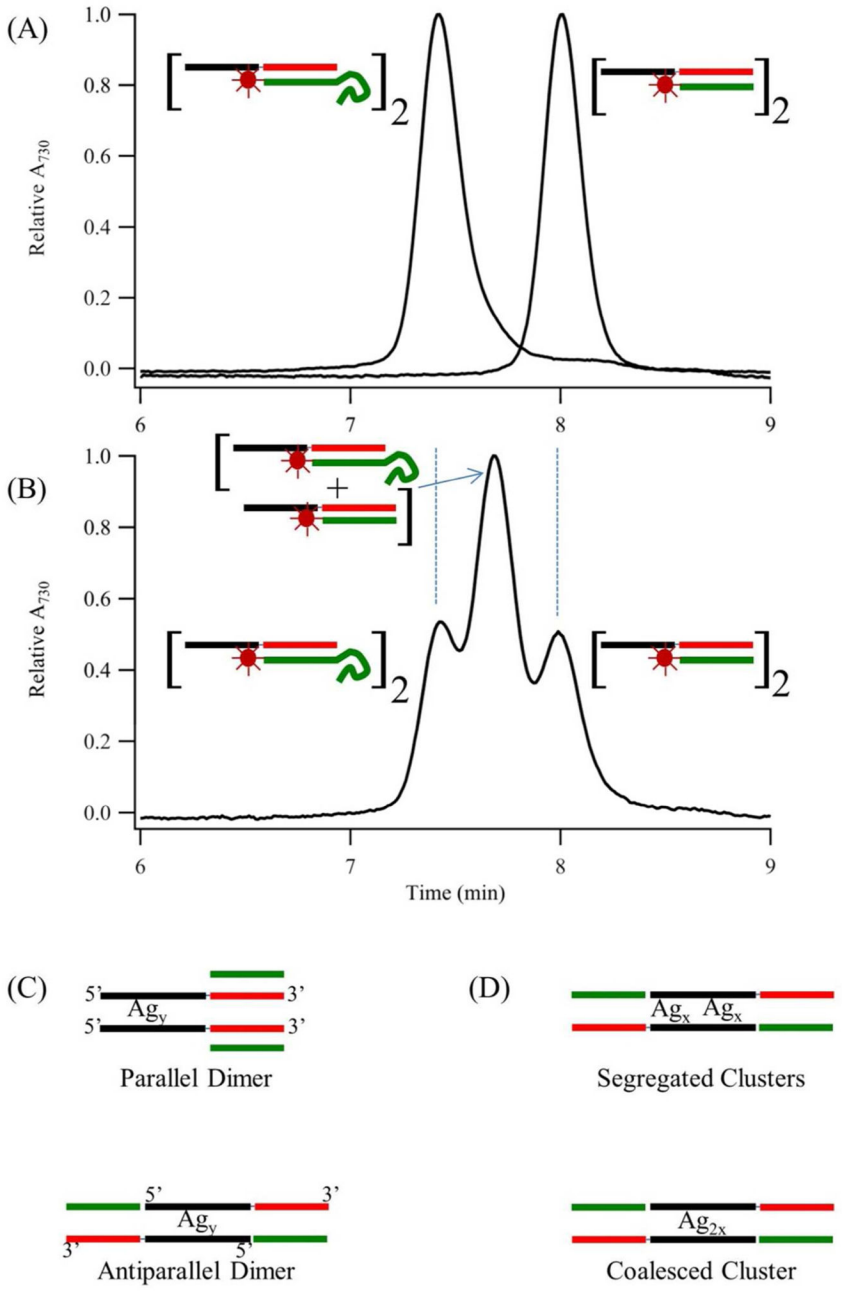

Figure 4.

Size exclusion chromatograms acquired by monitoring the cluster-specific absorbance at 730 nm and using two complementary strands without and with a 5′ dT_{10} appendage (solid green extension from the complementary strand). In the top panel, each complement yields a distinct peak with near-infrared absorption when it binds to the sensor strand, and the difference in retention times is due to a larger hydrodynamic radius associated with the thymine tail. In the bottom panel, a mixture of these two complements produces a triplet pattern, and the vertical lines show the correspondence between the control samples in the top panel and the outer peaks in the bottom panel. The intermediate peak is ascribed to an

aggregate incorporating both types of complements, and a statistically weighted pattern supports two equivalent binding sites in a crosslinked dimer. (C) Parallel and antiparallel models for the organization of the hybridized dimeric sensors, with the polarity of the sensor strand indicated. The designation Ag_y represents either case in Figure 4D for the cluster organization. The color scheme for the components of this sensor follows that used in Figure 1. (D) Models for the cluster organization based on distinct vs. coalesced clusters, in which $x \approx 11$ silver atoms.